2024 American Control Conference (ACC)
July 8-12, 2024. Toronto, Canada

Short-term wind forecasting using surface pressure measurements

Seyedalireza Abootorabi, Stefano Leonardi, Mario Rotea, and Armin Zare

Abstract— **We propose a short-term wind forecasting framework that enables model-based control systems to preemptively adapt ahead of atmospheric variations in improving turbine efficiency and reducing structural loads and failures. Our approach relies on a combination of linear stochastic estimation and Kalman filtering algorithms to assimilate and process real-time nacelle-mounted anemometer and surface air-pressure readings with the predictions of a stochastic reduced-order model of the hub-height velocity field. Our results serve as a proof of concept for a wind forecasting strategy based on ground-level pressure sensor measurements.**

Index Terms— **Kalman filter, optimal estimation, stochastically forced Navier-Stokes, wake modeling, wind energy.**

I. Introduction

Adjustments to the turbine blade pitch, generator torque, and nacelle direction (yaw) are conventional strategies for increasing energy production and lowering operation and maintenance costs by countering the effects of atmospheric variability on wind plants. However, in the absence of effective short-term forecasting tools, almost all modern-day plants rely on data collected at or just behind the wind turbine to adjust their settings, and consequently could lag optimal operation conditions. This motivates the development of short-term wind forecasting tools for estimating changes to the rotor effective velocity due to atmospheric variations.

Efforts have been made to use data-assimilation for estimating the direction and speed of wind. These have primarily relied on predictions of 2D models of the hub-height velocity field corrected by the entrainment of downwind velocity measurements (e.g., [1]–[3]. The practicality of such approaches is, however, challenged by: (i) dimensional and dynamic complexities [1], [2]; and (ii) lack of robustness and generalizability in the case of data-driven estimation [4], [5]. To address these challenges, we propose an estimation framework that relies on the sequential self-correcting property of the Kalman filter in assimilating measurements from ground-level air-pressure sensors that are distributed across the farm and predictions of a particular class of low-complexity physics-based models, i.e., the stochastically forced linearized Navier-Stokes (NS) equations [6]–[9].

This work was supported in part by the National Science Foundation under awards 1916715 and 1916776 (I/UCRC for Wind Energy, Science, Technology, and Research) and from the members of WindSTAR I/UCRC. Any opinions, findings, and conclusions or recommendations expressed in this material are those of the author(s) and do not necessarily reflect the views of the National Science Foundation or the sponsors.

S. Abootorabi, S. Leonardi, M. A. Rotea, and A. Zare are with the UTD Wind Energy Center and the Department of Mechanical Engineering, University of Texas at Dallas, Richardson, TX 75080, USA.
Email: armin.zare@utdallas.edu

Engineering wake models provide analytical expressions for the long-time geometric expansion of turbine wakes under steady atmospheric conditions [10], [11]. As such static models do not account for atmospheric turbulence, they fall short of capturing the time-varying features of the waked velocity field, and thus, misrepresent wake recovery. To overcome these shortcomings, contributions have been made to add a degree of dynamics, e.g., the dynamic wake-meandering model [12] or the dynamic extension of the Park model [13]. In [14], the stochastic dynamical modeling framework of [7], [15]–[17] was utilized for shaping a stochastic source of excitation into the linearized NS equations around the Gaussian wake profile [18], [19]. This approach results in fluctuation dynamics that are statistically consistent (at the level of second-order statistics) with a high-fidelity large-eddy simulation (LES). It also provides a solution to Kalman filtering in the presence of colored-in-time process noise with unknown dynamics [20].

In this paper, we build on the predictive capability of said stochastic models and devise Kalman filters that account for changes in hub-height velocity fluctuations by assimilating model-based predictions with measured variations in air-pressure from the ground. We consider a 2D model of hub-height velocity and utilize a data-driven projection scheme to map the resulting pressure at hub height to the ground when updating the posterior estimate (Fig. 1). We use LES-generated flow fields [21] within a cascade of 2 turbines to compare the performances of the linearized Kalman filter (LKF), the extended Kalman filter (EKF), and the unscented Kalman filter (UKF).

The paper is organized as follows. In Sec. II, we formulate the problem and present our approach. In Sec. III, we summarize our method in constructing a prior linear-time invariant (LTI) model that is statistically consistent with high-fidelity LES. In Sec. IV, we provide details of Kalman filtering algorithms. In Sec. V, we compare the performance of various Kalman filters in estimating hub-height velocity variations based on ground pressure measurements. We provide concluding remarks in Sec. VI.

II. Problem Formulation and Approach

The dynamics of the flow field impinging on a wind farm is given by the nonlinear NS and continuity equations

$$\begin{aligned} \partial_t \mathbf{u} &= f(\mathbf{u}, P) \\ 0 &= \nabla \cdot \mathbf{u} \end{aligned} \tag{1}$$

where t is time, $\mathbf{u}(\mathbf{x}, t)$ consists of the three components of the velocity field with $\mathbf{x} = [\, x \;\; y \;\; z \,]^T$ denoting the vector of spatial coordinates in streamwise (x), wall-normal (y), and

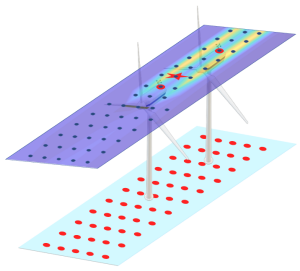

Fig. 1. The computational (top) and sensing (bottom) planes within our estimation framework. Blue dots indicate the training points in stochastic modeling, while red dots represent sensor locations. The estimation point is denoted by the red star in the wake of the leading turbine.

spanwise (z) directions, P is the pressure, and ∇ is the gradient operator. Given a set of partially available steady-state correlations of the velocity field, we are interested in constructing an estimator that: (i) in the absence of innovations, provides statistical consistency with the original nonlinear model (1); and (ii) tracks velocity variations at the hub-height of wind turbines based on real-time measurements from ground-level air-pressure sensors and nacelle-mounted anemometers. The first feature is motivated by the desire to account for colored-in-time process noise and the second aims to support a recently proposed sensing technology [22] for short-term wind forecasting that is cheaper than Doppler LiDAR. To these ends, we propose a Kalman filter-based estimation framework that relies on two pillars:

- Stochastic dynamical modeling of the hub-height velocity field using the linearized NS equations;
- Data-driven inference of hub-height pressure from ground-level pressure measurements.

The first addresses the necessity for models of reduced complexity for short-term forecasting and is based on the predictive capability of the stochastically forced linearized NS equations around static solutions of engineering wake models [14], [23]. The process noise that drives the linearized dynamics is identified via convex optimization to ensure second-order statistical consistency with high-fidelity LES of the wind farm flow [20]. The second pillar is based on the construction of a data-driven kernel transfer function for projecting hub-height pressure to the ground (Fig. 1). Building on these elements, we compare the performance of various Kalman filtering algorithms.

III. Stochastic Dynamical Modeling

In this section, we provide details of the 2D model we use for flow estimation. Let the total wind velocity $\mathbf{u}$ in the 2D horizontal plane at hub-height be composed of a static base flow $\bar{\mathbf{u}}$ and zero-mean fluctuations $\mathbf{v}$, i.e., $\mathbf{u} = \bar{\mathbf{u}} + \mathbf{v}$, where $\mathbf{v} = [u \;\; w]^T$ consists of the streamwise u and spanwise w velocity components. We consider a base flow that only consists of a streamwise component given by the engineering wake model of Bastankhah and Porté-Agel [18],

$$U(x,z) \;=\; U_\infty - U_\infty \left(1 - \sqrt{1 - \frac{C_T}{8\,\sigma_x^2}}\right) \mathrm{e}^{-\left(\frac{z}{2\,\sigma_x}\right)^2} \qquad (2)$$

which describes the waked velocity behind a turbine that is aligned with the free-stream velocity U_∞ (no yaw). Here, all length scales have been non-dimensionalized by the turbine diameter, C_T is the thrust coefficient, and $\sigma_x := k^\star x + 0.2\sqrt{\beta}$, where $k^\star$ is the wake growth rate and $\beta = (1 + \sqrt{1 - C_T})/(2\sqrt{1 - C_T})$. We then use linear superposition to capture velocity deficits in regions where turbine wakes overlap and assume the dynamics of fluctuations $\mathbf{v}$ are given by the stochastically forced linearized NS equations around the resulting velocity profile. A standard conversion for eliminating pressure p and finite-dimensional approximation of the differential operators yields the state-space representation

$$\dot{\mathbf{v}}(t) \;=\; A\,\mathbf{v}(t) \,+\, B\,\mathbf{d}(t) \qquad (3)$$

where velocity has been non-dimensionalized by the free-stream U_∞ and the state vector $\mathbf{v}$ contains velocity fluctuations over the 2D spatial domain; see [14, Appendix A] for details on dynamic matrices A and B. Here, $\mathbf{d}$ is a zero-mean stochastic process that triggers a statistical response from the linear dynamics and provides a degree of freedom for shaping the statistics of $\mathbf{v}$.

The performance of Kalman filters is influenced by the statistics of disturbance models we use to account for uncertainty [24], [25]. Recently, it has been shown that white-in-time process noise falls short in reproducing the statistical signature of the wind velocity especially in the wake of operating turbines [23], [26]. Alternatively, one may follow [26] in utilizing the optimization-based framework of Refs. [7], [16], [17] to identify the statistics of the colored-in-time input that ensure certain, more dominant, second-order statistics of the velocity field are matched. Access to wind speed data in the wind energy industry has grown remarkably in the past decades and such statistics could be computed from the result of high-fidelity simulations or field measurements. Herein, we specifically assume knowledge of a subset of second-order statistics of hub-height velocity upwind of the wind farm and in the wake region up to 4 diameters behind the turbines (Fig. 1). These velocity correlations correspond to entries on the diagonal of the steady-state covariance matrix $\mathbf{V} := \lim_{t\to\infty} \mathbf{E}[\mathbf{v}(t)\mathbf{v}^T(t)]$, which solves the Lyapunov-like equation [16], [27],

$$A\,\mathbf{V} \,+\, \mathbf{V}A^* \;\;=\;\; -\,B\,H^* \,-\, H\,B^* \qquad (4)$$

where the matrix H quantifies the cross-correlation between the input and the state [17, Appendix B], i.e., $H := \lim\limits_{t\to\infty} \mathbf{E}\,[\mathbf{v}(t)\mathbf{d}^*(t)] + B\Omega/2$. Coincidentally, it is this matrix that contains information on the coloring filter for generating the stochastic input $\mathbf{d}$ [16].

Matrix H and the input matrix B can be obtained from the solution of the covariance completion problem

$$\begin{aligned} \underset{\mathbf{V},\,Z}{\text{minimize}} \quad & -\log\det(\mathbf{V}) \,+\, \alpha\,\|Z\|_* \\ \text{subject to} \quad & A\,\mathbf{V} \,+\, \mathbf{V}A^* \,+\, Z \;=\; 0 \\ & \mathbf{V}_{i,j} \;=\; G_{i,j}, \quad \forall\, \{i,j\} \in \mathcal{I}. \end{aligned} \qquad (5)$$

This convex optimization problem solves for Hermitian matrices $\mathbf{V}$ and Z subject to two linear constrains that ensure

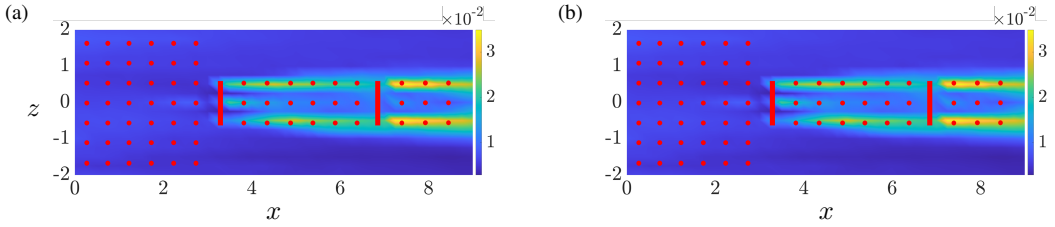

Fig. 2. Streamwise velocity variance calculated from LES results (left) and model (6) (right). The spatial positions of velocity correlations used to train the stochastic model are indicated by red dots, while turbine rotors are highlighted by thick red lines. The wind blows from left to right.

consistency with the assumed linear model via satisfaction of the Lyapunov-like equation (4) and the partially known velocity correlations; entries of G corresponding to the set of indices $\mathcal{I}$ represent partially available second-order statistics of the output $\mathbf{v}$. The objective function provides a weighted trade-off through determination of $\alpha > 0$ between the solution to a maximum-entropy problem, which uses the logarithmic barrier function to ensure positive definiteness of matrix $\mathbf{V}$, and a nuclear norm regularizer, which is used as a convex proxy for the rank function (see, e.g., [28]). It is desirable to regulate the rank of matrix Z as it bounds the number of independent input channels or columns in matrix B. Without this regularization, a full-rank matrix B permits colored-in-time input $\mathbf{d}$ to excite all degrees of freedom and completely overwrite the linearized dynamics A [16].

The solution Z to problem (5) can be decomposed into matrices B and H (cf. Eq. (4)) via spectral decomposition techniques, which in turn can be used to construct linear coloring filters that realize the input signal $\mathbf{d}$. Alternatively, the coloring filter can be absorbed in the LTI dynamics (3) in a standard manner yielding the dynamically modified state-space representation

$$\dot{\mathbf{v}}(t) \;=\; (A - B\,K_f)\,\mathbf{v}(t) \;+\; B\,\mathbf{w}(t). \tag{6}$$

Here, $\mathbf{w}$ is white noise and K_f is a parameter of the coloring filter with parameterization offered in [16, Sec. II.B]. Additional details on the choice of velocity correlations for best recovery, and the robustness of predictions to turbine yawing effects can be found in Refs. [14], [23].

Figure 2 demonstrates the performance of model (6) in recovering streamwise intensity at the hub-height of a turbine cascade. Red dots denote the location of the available correlations in the training dataset. In the absence of innovations, the identified colored process noise model ensures statistical consistency with an LES that leverages blade momentum element theory [21]. The close agreement of the predictions of our model and the result of LES in regions beyond the training dataset warrant its use for Kalman filtering.

IV. Kalman Filtering Algorithms

We use Kalman filters to update our model-based predictions of the hub-height velocity field in accordance with real-time readings of ground-level pressure sensors and nacelle-mounted anemometers that are affected by atmospheric variations. While the stochastic modeling step for obtaining the prior LTI model (6) is conducted in continuous time, we implement discrete-time analogues of conventional Kalman filters, namely, the LKF, the EKF, and the UKF, in our numerical experiments. These variants differ in handling the nonlinear measurement equation

$$\varphi(t) \;:=\; \begin{bmatrix} p_{\mathrm{g}}(t) \\ \mathbf{v}_{\mathrm{nacelle}}(t) \end{bmatrix} \;=\; \begin{bmatrix} \mathcal{H}_{\mathrm{gh}}\mathcal{P}(\mathbf{v}(t)) \\ E\,\mathbf{v}(t) \end{bmatrix} \;:=\; \mathcal{C}(\mathbf{v}(t)), \tag{7}$$

which establishes a nonlinear relation between hub-height velocity fluctuations $\mathbf{v}$ from model (6) and pressure on the ground p_{g}. Here, E is a matrix with the same number of rows as the number of nacelle-mounted anemometers. Each row of E has a 1 at the entry corresponding to the location of an anemometer and is otherwise zero. Moreover, $\mathcal{H}_{\mathrm{pg}}$ is a transfer kernel that projects hub-height pressure to the ground (Sec. IV) and $\mathcal{P}(\cdot)$ denotes the pressure Poisson equation

$$p \;=\; -\Delta^{-1}\left[\left(\frac{\partial u}{\partial x}\right)^2 + 2\,\frac{\partial u}{\partial z}\,\frac{\partial w}{\partial x} + \left(\frac{\partial w}{\partial z}\right)^2\right]. \tag{8}$$

The LKF employs the linearization of Eq. (7) around the initial state $\hat{\mathbf{v}}_0$; at each iteration k, the pressure on the ground is calculated from the velocity estimate at hub-height via

$$\begin{aligned} p_{\mathrm{g},k} \;&=\; \mathcal{H}_{\mathrm{gh}}\left(\frac{\partial \mathcal{P}}{\partial \mathbf{v}}\Big|_{\hat{\mathbf{v}}_0}\right)^T \hat{\mathbf{v}}_k \\ &=\; \mathcal{H}_{\mathrm{gh}}\begin{bmatrix} \dfrac{\partial \hat{u}_0}{\partial x}\dfrac{\partial}{\partial x} + \dfrac{\partial \hat{w}_0}{\partial x}\dfrac{\partial}{\partial z} \\ \dfrac{\partial \hat{u}_0}{\partial z}\dfrac{\partial}{\partial x} + \dfrac{\partial \hat{w}_0}{\partial z}\dfrac{\partial}{\partial z} \end{bmatrix}^T \begin{bmatrix} \hat{u}_k \\ \hat{w}_k \end{bmatrix} \end{aligned} \tag{9}$$

and follows the standard form of the optimal state estimator [29, Sec. 5.1], whereas the EKF and UKF respect the nonlinear evolution (7) by either iteratively linearizing around the current state estimate or averaging over an ensemble of trajectories resulting from a deterministic set of sigma points [29, Sec. 14].

For uncorrelated, white, zero-mean process $\mathbf{w}_k$ and measurement noise η_k with respective covariances $\Omega \succ 0$ and $R \succ 0$, Algorithm 1 summarizes the steps of the EKF in obtaining an estimate of the hub-height fluctuation field $\hat{\mathbf{v}}_k$. Here, $F := \mathrm{e}^{A_f \Delta t}$ and $G := (\mathrm{e}^{A_f \Delta t} - I)A_f^{-1}B$ with $A_f := A - BK_f$ (cf. Eq. (6)), I as the identity matrix, and Δt as the time step, L_k is the Kalman gain, $\Psi_k := \mathbf{E}[(\mathbf{v}_k - \hat{\mathbf{v}}_k)(\mathbf{v}_k - \hat{\mathbf{v}}_k)^T]$ is the covariance of the estimation error with $\mathbf{E}(\cdot)$ denoting the expected value, C_k is the finite-dimensional approximation of the linearized measurement

equation (Eq. (7)) around the Kalman filter estimate, i.e.,

$$C_k = \begin{pmatrix} \mathcal{H}_{\rm gh} \dfrac{\partial \mathcal{P}}{\partial \mathbf{v}}\Big|_{\hat{\mathbf{v}}_k} \\ E \end{pmatrix} \tag{10}$$
$$= \begin{pmatrix} 2\mathcal{H}_{\rm gh}\left[\dfrac{\partial \hat{u}_k}{\partial x}\dfrac{\partial}{\partial x} + \dfrac{\partial \hat{w}_k}{\partial x}\dfrac{\partial}{\partial z} \quad \dfrac{\partial \hat{u}_k}{\partial z}\dfrac{\partial}{\partial x} + \dfrac{\partial \hat{w}_k}{\partial z}\dfrac{\partial}{\partial z}\right] \\ E \end{pmatrix}$$

such that $\varphi_k = [\, p_{{\rm g},k} \;\; \mathbf{v}_{\rm nacelle} \,]^T = C_k \mathbf{v}_k$, and $\mathcal{I}_C$ is a set of indices corresponding to the measurements that are retained in the sensing architecture. We note that sensors may not be placed at all spatial locations throughout the farm and the set $\mathcal{I}_C$ allows for a selection of a subset of all possible spatial locations for the placement of sensors.

Algorithm 1 Extended Kalman Filter

input: F, G, Ω, R and $\mathcal{I}_c$
initialize: $\hat{\mathbf{v}}_0^+$ and $\Psi_{\mathbf{v},0}^+$
for $k = 1, 2, \ldots$

- linearize the output operator around the current estimate $\hat{\mathbf{v}}_{k-1}^+$ based on Eq. (10)
- retain the rows in C_k corresponding to $\mathcal{I}_c$

$R_k = I_{{\rm card}(\mathcal{I}_c)}$

$$\Psi_{\mathbf{v},k}^- = F\,\Psi_{\mathbf{v},k-1}^+ F^T + G\,\Omega G^T$$
$$\hat{\mathbf{v}}_k^- = F\,\hat{\mathbf{v}}_{k-1}^+$$
$$L_k = \Psi_{\mathbf{v},k}^- C_k^T \left(C_k\,\Psi_{\mathbf{v},k}^- C_k^T + R\right)^{-1}$$
$$\hat{\mathbf{v}}_k^+ = \hat{\mathbf{v}}_k^- + L_k\left(\varphi_k - \mathcal{C}(\hat{\mathbf{v}}_k^-)\right)$$
$$\Psi_{\mathbf{v},k}^+ = (I - L_k C_k)\,\Psi_{\mathbf{v},k}^- (I - L_k C_k)^T + L_k R L_k^T$$

endfor
output: $\hat{\mathbf{v}}_k^+$ and $\Psi_{\mathbf{v},k}^+$ as the posterior estimates of the velocity field and the covariance of the error

While the EKF is the most widely used nonlinear state estimation method, it comes with errors due to linearization. One way to mitigate this issue is to use the UKF, which does not involve linearization of the $\mathcal{C}(\cdot)$ operator, but instead comes with the added computational cost of marching a large number (typically, double the number of states) of sigma points and averaging over the ensemble of estimation errors. In Sec. V, we also present the result of the UKF algorithm, but refrain from a comprehensive presentation for brevity; see [29, Sec. 14.3] for details.

Pressure projection via linear stochastic estimation

The existence of coherent motions in wall-bounded flows can result in strong two-point correlations of flow quantities, e.g., pressure and velocity, between points that are near the wall and away from it [30]. This motivates the use of linear stochastic estimators for projecting wall-separated measurements to the near-wall region (and vice versa) using normalized variants of such two-point correlations [31]. In this vein, near-wall pressure fluctuations have been shown to maintain higher levels of correlation with wall-separated regions [31]. Assuming a correlation between pressure at hub-height $p_{\rm h}$ and on the ground, an estimate of ground-level pressure $p_{\rm g}$ can be provided through the linear transformation

$$p_{\rm g}(x,z) \;=\; \mathcal{H}_{\rm gh}(x,z)\, p_{\rm h}(x,z). \tag{11}$$

The pressure at hub-height is assumed to be computed using Eq. (8) and the prediction of the linear stochastic model (6), and $\mathcal{H}_{\rm gh}$ is the normalized two-point correlation,

$$\mathcal{H}_{\rm gh}(x,z) \;:=\; \frac{\langle p_{\rm h}(x,z)\, p_{\rm g}(x,z)\rangle}{\langle p_{\rm h}(x,z)\, p_{\rm h}(x,z)\rangle}$$

that is trained using a time-resolved pressure field resulting from high-fidelity simulations or field measurements. In this definition, $\langle\cdot\rangle$ is an expectation operator computed over a sufficiently long time window to ensure statistical convergence in $\mathcal{H}_{\rm gh}$. Figure 3 compares the ground-level pressure across a two-turbine farm resulting from LES (Fig. 3(a)) with the projection of hub-height pressure using Eq. (11) (Fig. 3(b)). It is evident that the projected pressure field captures the dominant pressure variations on the ground, which justifies the use of linear stochastic estimation for our purposes.

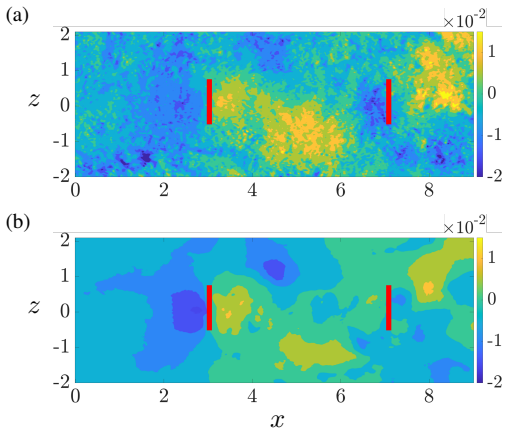

Fig. 3. Snapshots showing the ground-level pressure field from LES (left) and the projection of LES-based hub-height pressure resulting from Eq. (11) (right) at the same time instant. Turbine rotors are marked by red lines and the wind blows from left to right.

V. Numerical Experiments

We present results for flow fluctuation estimation in a wind farm with two turbines using the proposed estimation framework. We consider a horizontal domain at hub-height with $x \in [0\;\; 9]$ and $z \in [-2, 2]$ and turbines of unit diameter located at $(x, z) = (3, 0)$ and $(7, 0)$ (Fig. 1). Following the LES that generated the training dataset, the farm is impacted by turbulent flow with Reynolds number 10^8; see [14, Sec. 5.1] for details. We use a uniform grid with $\Delta x = \Delta z = 0.25$ and a second-order central difference scheme to discretize the computational grid and differential operators in the linearized NS equations, which leads to $\mathbf{v} \in \mathbb{R}^{1462\times 1}$ in model (6). The modification to the linearized dynamic generator is obtained via the modeling framework summarized in Sec. III to achieve consistency with LES in matching velocity correlations at locations highlighted

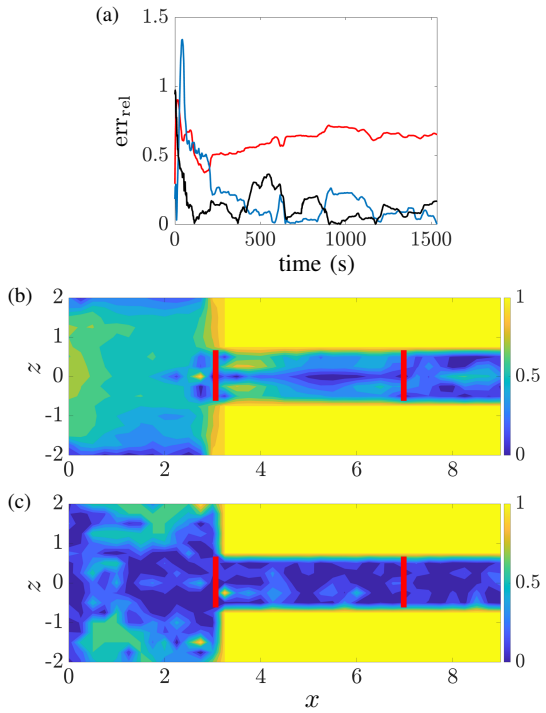

Fig. 4. (a) Relative error in estimating the velocity variance (Eq. (12)) at $(x, z) = (4, 0)$: LKF (red), EKF (blue), and UKF (black). (b,c) Spatial variation of $\mathrm{err}_{\mathrm{rel}}$ (Eq. (12)) at $t = 1536$ sec over the 2D domain obtained by EKF (b) and UKF (c). Turbine rotors are marked by red lines, and the wind blows from left to right.

in Fig. 2. To quantify performance, we propose two error metrics: the first is a running relative error in matching the variance of streamwise velocity at hub-height, i.e.,

$$\mathrm{err}_{\mathrm{rel}}(\mathbf{x}, t) = \frac{\left| \int_0^t \left(u^2_{\mathrm{LES}}(\mathbf{x}, \tau) - \hat{u}^2(\mathbf{x}, \tau) \right) \mathrm{d}\tau \right|}{\int_0^t u^2_{\mathrm{LES}}(\mathbf{x}, \tau) \mathrm{d}\tau} \quad (12)$$

and the second is the error in matching the streamwise velocity normalized by the local base flow U, i.e.,

$$\mathrm{err}_{\mathrm{norm}}(\mathbf{x}, t) = \frac{|u_{\mathrm{LES}}(\mathbf{x}, t) - \hat{u}(\mathbf{x}, t)|}{U(\mathbf{x})}. \quad (13)$$

Normalization by the base flow gives more weight to dynamically significant regions of the flow (e.g., within the turbine wakes) that may be more difficult to estimate.

Figure 4(a) shows the relative statistical error $\mathrm{err}_{\mathrm{rel}}$ at $(x, z) = (4, 0)$ behind the leading turbine as a function of time for all the Kalman filters. For both EKF and UKF, the relative error goes through transient spikes while overall decreasing. This is not the case for the LKF for which $\mathrm{err}_{\mathrm{rel}}$ remains above 60%. Due to this high error, we exclude results of the LKF from the remainder of this section. Figures 4(b,c) compare the statistical errors obtained using the EKF and the UKF at $t = 1536$ sec over the 2D domain. While the UKF generally outperforms the EKF in capturing the velocity variance, the EKF performs reasonably well in the wake region behind the first turbine, which is of importance in forecasting the wind that will impinge on the second row of turbines. It is noteworthy that the EKF achieves this level of accuracy in significantly less

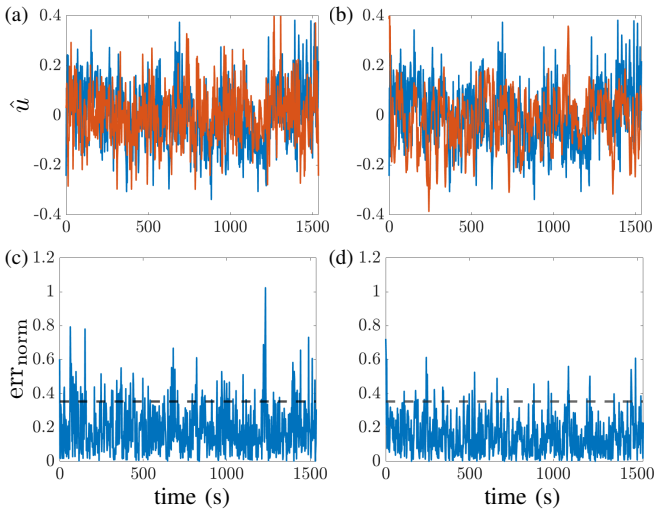

Fig. 5. Top row: Fluctuations in streamwise velocity at $(x, z) = (4, 0)$ obtained from LES (blue) and Kalman filters (orange). Bottom row: Changes in the normalized error $\mathrm{err}_{\mathrm{norm}}$ when estimating streamwise velocity fluctuations at $(x, z) = (4, 0)$. (a,c) EKF results and (b,d) UKF results. The black dashed lines indicate the 3σ error boundaries.

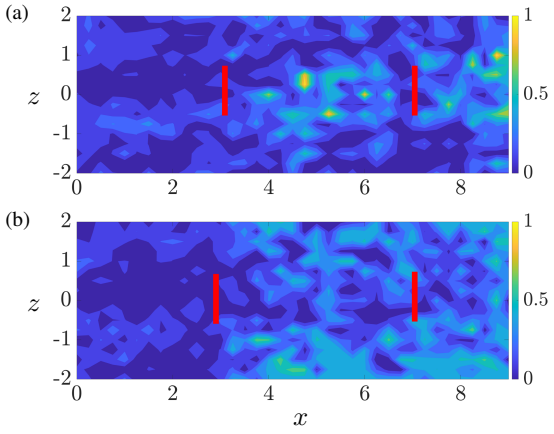

Fig. 6. Colormaps of the normalized error (Eq. (13)) at $t = 1536$ seconds across the 2D domain using (a) EKF; and (b) UKF algorithms. Turbine rotors are marked by red lines, and the wind blows from left to right.

computational time (4 minutes vs approximately 2 hours). We note that the sharp transition between regions with low and high $\mathrm{err}_{\mathrm{rel}}$ in Figs. 4(b,c) highlights the significance of stochastic modeling phase and the locations from which training data were collected (cf. Fig. 2).

Figures 5(a,b) show the time evolution of EKF- and UKF-based velocity estimates (blue color) plotted against the LES data (orange color) at $(x, z) = (4, 0)$. In Figs. 5(c,d) the normalized errors (Eq. (13)) have been plotted for the EKF and UKF together with the 3σ error bounds. While these plots demonstrate an advantage in using the UKF, they are also indicative of reasonably good estimation levels and quick recovery to sudden changes when using the EKF. Finally, Fig. 6 shows the contour map of the normalized error (Eq. (13)) at $t = 1536$ seconds over the 2D domain at hub height. As expected, the UKF outperforms the EKF in most of the domain, especially in the wake region, where turbulence intensity is higher.

VI. Concluding remarks

We study the efficacy of various Kalman filtering algorithms in estimating changes in hub-height wind velocity due to LES-generated atmospheric variations. Our estimation algorithms rely on a stochastic dynamical model of hub-height velocity and a projection strategy for mapping pressure changes from the hub-height to the ground. For the first, we use the stochastically forced linearized NS equations around 2D velocity profiles provided by static engineering wake models. The input stochastic excitation, which represents the process noise in Kalman filters, is designed via inverse modeling to match statistical signatures of the LES-based velocity field at hub-height. Assuming access to ground pressure throughout the entire domain, we evaluated the performance of the LKF, EKF, and UKF algorithms in estimating the wind velocity and its variance relative to the result of LES. Our results serve as a proof of concept for short-term wind forecasting based on ground-level pressure sensor measurements as an alternative to those that rely on LiDAR scanners. Despite the superior performance of the UKF, given its high computational cost, the EKF can be considered as a potential candidate for further development of such forecasting tools. Our ongoing work focuses on identifying regions of the farm that are most important for the placement of pressure sensors via optimal sensor selection (e.g. [32], [33]) and studying the performance of our forecasting tool under varying nominal wind speeds where robust Kalman filtering techniques (e.g., [34]) could provide additional generalizability.

Acknowledgments

The Office of Information Technology Cyberinfrastructure Research Computing (CIRC) at The University of Texas at Dallas and the Texas Advanced Computing Center are acknowledged for providing computing resources.

References

[1] B. M. Doekemeijer, J.-W. van Wingerden, S. Boersma, and L. Y. Pao, "Enhanced Kalman filtering for a 2D CFD NS wind farm flow model," in *J. Phys.: Conference Series*, vol. 753, no. 5, 2016, p. 052015.

[2] B. M. Doekemeijer, S. Boersma, L. Y. Pao, T. Knudsen, and J.-W. van Wingerden, "Online model calibration for a simplified les model in pursuit of real-time closed-loop wind farm control," *Wind Energy Sci.*, vol. 3, no. 2, pp. 749–765, 2018.

[3] C. R. Shapiro, G. M. Starke, C. Meneveau, and D. F. Gayme, "A wake modeling paradigm for wind farm design and control," *Energies*, vol. 12, no. 15, p. 2956, 2019.

[4] G. V. Iungo, C. Santoni-Ortiz, M. Abkar, F. Porté-Agel, M. R. A, and S. Leonardi, "Data-driven reduced order model for prediction of wind turbine wakes," in *J. Phys.: Conference Series*, vol. 625, no. 1, 2015, p. 012009.

[5] M. Sinner, L. Pao, and J. King, "Estimation of large-scale wind field characteristics using supervisory control and data acquisition measurements," in *2020 American Control Conference (ACC)*, 2020, pp. 2357–2362.

[6] M. R. Jovanovic and B. Bamieh, "Componentwise energy amplification in channel flows," *J. Fluid Mech.*, vol. 534, pp. 145–183, July 2005.

[7] A. Zare, T. T. Georgiou, and M. R. Jovanovic, "Stochastic dynamical modeling of turbulent flows," *Annu. Rev. Control Robot. Auton. Syst.*, vol. 3, pp. 195–219, 2020.

[8] M. R. Jovanović, "From bypass transition to flow control and data-driven turbulence modeling: An input-output viewpoint," *Annu. Rev. Fluid Mech.*, vol. 53, no. 1, pp. 311–345, January 2021.

[9] S. Abootorabi and A. Zare, "Model-based spectral coherence analysis," *J. Fluid Mech.*, vol. 958, p. A16 (32 pages), March 2023.

[10] N. O. Jensen, "A note on wind generator interaction," 1983.

[11] S. Frandsen, R. Barthelmie, S. Pryor, O. Rathmann, S. Larsen, J. Højstrup, and M. Thøgersen, "Analytical modeling of wind speed deficit in large offshore wind farms," *Wind Energy: An International Journal for Progress and Applications in Wind Power Conversion Technology*, vol. 9, no. 1-2, pp. 39–53, 2006.

[12] G. C. Larsen, H. A. Madsen, K. Thomsen, and T. J. Larsen, "Wake meandering: a pragmatic approach," *Wind Energy*, vol. 11, no. 4, pp. 377–395, 2008.

[13] J. Annoni, K. Howard, P. Seiler, and M. Guala, "An experimental investigation on the effect of individual turbine control on wind farm dynamics," *Wind Energy*, vol. 19, no. 8, pp. 1453–1467, 2016.

[14] A. H. Bhatt, F. Bernardoni, S. Leonardi, and A. Zare, "Stochastic dynamical wake modeling for wind farms," *arXiv preprint arXiv:2208.12196*, 2022.

[15] A. Zare, M. R. Jovanovic, and T. T. Georgiou, "Completion of partially known turbulent flow statistics," in *Proceedings of the 2014 American Control Conference*, 2014, pp. 1680–1685.

[16] A. Zare, Y. Chen, M. R. Jovanovic, and T. T. Georgiou, "Low-complexity modeling of partially available second-order statistics: theory and an efficient matrix completion algorithm," *IEEE Trans. Automat. Control*, vol. 62, no. 3, pp. 1368–1383, 2017.

[17] A. Zare, M. R. Jovanovic, and T. T. Georgiou, "Colour of turbulence," *J. Fluid Mech.*, vol. 812, pp. 636–680, 2017.

[18] M. Bastankhah and F. Porté-Agel, "A new analytical model for wind-turbine wakes," *Renewable energy*, vol. 70, pp. 116–123, 2014.

[19] M. Bastankhah and F. Porté-Agel, "Experimental and theoretical study of wind turbine wakes in yawed conditions," *J. Fluid Mech.*, vol. 806, pp. 506–541, 2016.

[20] A. Zare, "Data-enhanced kalman filtering of colored process noise," in *Proceedings of the 60th IEEE Conference on Decision and Control*, 2021, pp. 6603–6607.

[21] C. Santoni, U. Ciri, M. Rotea, and S. Leonardi, "Development of a high fidelity CFD code for wind farm control," in *2015 American Control Conference (ACC)*, 2015, pp. 1715–1720.

[22] "Windscape AI," https://windscape.ai/, accessed: 2023-09-13.

[23] M. Rodrigues, N. A. Burgess, A. H. Bhatt, S. Leonardi, and A. Zare, "Robustness of two-dimensional stochastic dynamical wake models for yawed wind turbines," in *Proceedings of the 2023 American Control Conference*, 2023, pp. 818–823.

[24] J. Hœpffner, M. Chevalier, T. R. Bewley, and D. S. Henningson, "State estimation in wall-bounded flow systems. Part 1. Perturbed laminar flows," *J. Fluid Mech.*, vol. 534, pp. 263–294, 2005.

[25] M. Chevalier, J. Hœpffner, T. R. Bewley, and D. S. Henningson, "State estimation in wall-bounded flow systems. Part 2. Turbulent flows," *J. Fluid Mech.*, vol. 552, pp. 167–187, 2006.

[26] A. H. Bhatt, M. Rodrigues, F. Bernardoni, S. Leonardi, and A. Zare, "Stochastic dynamical modeling of wind farm turbulence," *Energies*, vol. 16, no. 19, p. 6908 (24 pages), September 2023.

[27] T. T. Georgiou, "The structure of state covariances and its relation to the power spectrum of the input," *IEEE Trans. Autom. Control*, vol. 47, no. 7, pp. 1056–1066, 2002.

[28] M. Fazel, "Matrix rank minimization with applications," Ph.D. dissertation, Stanford University, 2002.

[29] D. Simon, *Optimal state estimation: Kalman, H infinity, and nonlinear approaches*. John Wiley & Sons, 2006.

[30] I. Marusic and J. P. Monty, "Attached eddy model of wall turbulence," *J. Fluid Mech.*, vol. 51, pp. 49–74, 2019.

[31] W. J. Baars, G. Dacome, and M. Lee, "Wall-pressure–velocity coupling in high-reynolds number wall-bounded turbulence," *arXiv preprint arXiv:2307.06449*, 2023.

[32] A. Zare and M. R. Jovanovic, "Optimal sensor selection via proximal optimization algorithms," in *Proceedings of the 57th IEEE Conference on Decision and Control*, 2018, pp. 6514–6519.

[33] A. Zare, H. Mohammadi, N. K. Dhingra, T. T. Georgiou, and M. R. Jovanović, "Proximal algorithms for large-scale statistical modeling and sensor/actuator selection," *IEEE Trans. Automat. Control*, vol. 65, no. 8, pp. 3441–3456, 2020.

[34] X. Kai, C. Wei, and L. Liu, "Robust extended kalman filtering for nonlinear systems with stochastic uncertainties," *IEEE Trans. Syst. Man. Cybern.*, vol. 40, no. 2, pp. 399–405, 2009.